3D numerical modelling of braided channel formation

Nils Reidar B. Olsen

Department of Civil and Environmental Engineering, The Norwegian University of Science and Technology, Norway

ABSTRACT

A numerical model was used to compute the formation of a braided channel system. The model calculated the water flow field from the fully 3D Navier-Stokes equations on a non-orthogonal unstructured adaptive grid. The sediment transport was computed from the Engelund-Hansen formula. A free surface algorithm based on local pressure gradients was used. The model was applied to an idealized geometry of an initially straight alluvial channel, where the evolution of the braided channel system over time was computed. The complex processes and geometry for this case made it very well suited for testing the numerical model. The purpose of the study was also to explain avulsion processes of a braided river in more detail. Figures are presented with water depth, velocity, water level and secondary currents during an avulsion. The effect of the water level changes and the secondary currents are shown. The geometry, sediment size and water discharge used in the numerical model was identical to a laboratory study. Reasonable agreement was found when comparing the active braiding intensity (BI_A) computed by the numerical model with measurements from the flume experiment. Parameter tests include sediment transport formula, grid size, secondary current damping and grid parameters related to wetting/drying. The results using the Engelund-Hansen formula show a higher degree of braiding than the van Rijn or Mayer-Peter Müller formula. The secondary current strength is also shown to be very important for the braiding process and the BI_A values.

1. Introduction

A braided river consists of multiple channels that run parallel, where the channels are interconnected with bifurcations and confluences (Schumm et al., 1987). The geometry of the braided system changes over time, as some channels move laterally, some disappear and new branches are formed. The complexity of the geometry and its changes over time makes the braided channel difficult to model from a numerical point of view. It is therefore well suited for testing new algorithms for modelling sediment transport in natural rivers. This is one of the main motivations for focusing on braided rivers in the current study.

Braiding occurs in many natural river systems and has been the focus of a number of studies in the science of geomorphology (Hooke, 2004; van Dijk et al., 2014; Javernick et al., 2016). A motivation factor for studying braided channels in water engineering is their emergence during dam removal (Randle et al., 2015) and reservoir flushing (Haun and Olsen, 2012). When the water level in a reservoir is lowered, a braided channel can form and increase the effective width where sediments can be eroded. A larger volume of sand and silt can then be eroded from the reservoir than if only a single deep channel would have formed. This has economical implications for sediment

management. The braiding of a river is therefore of special engineering interest when studying reservoir flushing or effects of a dam removal.

Early work on braided rivers was carried out using physical model studies, for example Einstein and Shen (1964), who studied the effect of the Froude number on the formation of meanders. They also looked at how rough side banks would affect the erosion pattern of the meandering channel. Engelund and Skovgaard (1973) carried out a mathematical stability analysis of the momentum equations and sediment transport equations. The resulting amplification factor was connected to the wavelengths of the meanders. A recent study of meandering channels was carried out by da Silva and Ebrahimi (2017), presenting data from laboratory studies together with detailed descriptions of the flow and sediment transport physics.

Ferguson (1993) stated that numerical models have the potential to explain the processes of a braided river system. The growth in computing power over recent decades has made it possible to model water flow, sediment transport and morphological changes directly (Baranya et al., 2018; Xie et al., 2019). This can be done in one, two or three dimensions (Parsapour-Moghaddam and Rennie, 2017). The two and three-dimensional models show most promise because of the complexity of the braided river geometry. The technology behind such models is often called computational fluid dynamics (CFD), where the shallow-water equations or the Navier-Stokes equations are solved (Kim et al., 2020). A CFD model for a braided river requires algorithms for how to

incorporate laterally moving channels in the grid through a wetting/drying process (Khosronejad et al., 2019).

Two-dimensional models have been used by a number of researchers to compute vertical and lateral changes in rivers. Lotsari et al. (2014) computed the channel pattern changes over a year in the braided section of the Tana River in Norway using the 2D model TUFLOW. The results were compared with field observations. Williams et al. (2016) used a 2D version of Delft3D to compute the changes in a braided river on New Zealand, during a two-day high-flow event. The changes in the bed features were reasonably well reproduced, together with the volume of eroded and deposited sediments. Both these studies started the computation with a naturally braided geometry. A different initial boundary condition was used by other researchers, starting with a straight channel and looking at how it evolved into a braided system over time. Such physical model studies are well suited to test a numerical model. Jang and Shimizu (2005) computed the formation of a braided channel in a laboratory flume and compared the results with measurements. A structured grid that moved laterally according to the bank erosion was used. Good agreement was found between the results from the computations and the measurements for the channel wavelength and width. Schuurman et al. (2016) used two 2D models, Delft3D and Nays2D together with one 1D model to compute the formation of meandering and braided channel systems. They compared the results with empirical formulas for meander and bar lengths. Perturbations of the inflowing sediments were studied and found to be important. Rousseau et al. (2016) tested six 2D and 3D CFD models on three meandering channels with different sinuosity. Lateral movements of the geometries were not computed. The models gave varying accuracy, but the authors did not find any model that gave better results than the others. The numerical models usually include a substantial number of formulas and algorithms to take different fluid and sediment transport phenomena into account. Then it is necessary to have detailed knowledge about each model to be able to choose the most appropriate options.

Sun et al. (2015) used a 2D model to compute the same case as the current study: a braided flume experiment by Egozi and Ashmore (2009). Only the first 70 h of the 210 h physical laboratory experiment were computed, where the water discharge was kept constant. The computed total braiding intensity compared well with the measurements. Yang et al. (2017) used a similar numerical model to compute 140 h of the 210 h experiment.

The flow in river bends usually includes secondary currents causing the sediment to move towards the inside of bends. The process is important for the formation and development of meandering channels. A 2D model is not able to compute this 3D effect directly, but must rely on empirical formulas for the secondary currents. These formulas are usually in the form of a constant, K_1, multiplied with the water depth, h, and divided by the streamline curvature, R:

$$\tan \delta = -\frac{K_1 h}{R} \tag{1}$$

The angle between the depth-averaged velocity and the sediment velocity vector is denoted as δ.

A concern is how to choose the value of the constant K_1. This can be varied as a calibration parameter. Many researchers have used a value of seven (Jang and Shimizu, 2005; Sun et al., 2015, Langendoen et al., 2016). It is also possible to use a formula for K_1 that includes several constants and the friction factor of the bed (Lotsari et al., 2014; Li and Millar, 2011). Another problem with a 2D approach is that a secondary current may form at one bend and continue farther downstream of the bend (Stoesser et al., 2010; da Silva and Ebrahimi, 2017). There it still may have an effect on the sedimentation/erosion process. A 2D model would not be able to replicate this process, as the secondary current is only a function of the local depth-averaged streamline curvature. A 3D numerical model solves both these problems by computing the

secondary current directly from the Navier-Stokes equations. The downstream transport of the transverse circulation pattern is computed directly by the model.

Another concern with the 2D models is the computation of the turbulence. A zero-equation model is often used such as, for example, the following formula (Jang and Shimizu, 2005):

$$v_T = K_2 h u_* \tag{2}$$

The eddy-viscosity, v_T, is computed as a function of the water depth and the shear velocity, u_*, multiplied by a constant, K_2. This constant can be used as a calibration parameter. The approach assumes that the turbulence is in local equilibrium in each cell. Turbulence that is produced in an upstream cell and transported downstream is not taken into account. A fully 3D numerical model most often computes the turbulence using a more advanced approach, for example the k-epsilon model (Launder and Spalding, 1974). This model solves partial differential equations for the turbulence, which allows it to be transported with the flow.

Three-dimensional numerical morphological models have been used previously by Olsen (2003) to model formation of a meandering river. Another example is Liedermann et al. (2013), who used a fully 3D model to compute the movement of sediment particles in the Danube River. Fischer-Antze et al. (2008) also modelled a reach of the Danube River with a 3D model and compared the results with measured bed level changes during a large flood. Zinke et al. (2011) used a 3D model to compute sediment deposition on the vegetated banks in the braided delta of Lake Øyern in Norway. Changes in the main braiding pattern of the delta were, however, not computed.

The novelty of the present paper lies in the computation of a braided channel formation using a fully 3D numerical model, which uses an advanced turbulence model and computes the secondary currents directly. The results are compared with data from a physical model study, showing that the numerical model can reproduce the most important processes in the evolution of the braided system. This is also one of the aims of the current study. Another aim is to give additional insight into the physics of the avulsion process, which is important in the braiding process. Although physical model studies and field observations can give information about the braiding pattern evolution, a numerical model can still provide additional insight. The secondary currents are important for the lateral movement of a meandering river or a braided river branch. The strength of the secondary current is difficult to measure in a physical model of a braided river, as the vertical dimensions are small. It is also not straightforward to measure secondary currents in the field. A numerical model will easily produce figures of secondary current distributions, water depths, velocities and water surface elevations over time. This information enables the numerical model to explain more details of the processes of the braiding system, including avulsions. An example is given in the current article.

2. Physical model study

Physical models have a long tradition of being used in explaining geomorphological processes (Schumm et al., 1987). Laboratory models of braided rivers have been used by many researchers (Ettema et al., 2016; Bertoldi et al., 2014). The current study tests the numerical model against data from a flume study by Egozi and Ashmore (2009). An 18 m long and 3 m wide flume filled with sand was used. The slope of the flume was 1.5%. A 0.5 m wide and 1.5 cm deep channel was excavated in the middle of the flume before the experiment started. The sand had an average diameter of 1.2 mm, and a d_{90} of 3.6 mm. The sediment was recirculated during the experiment. The water discharge was varied in three stages. A constant discharge of 1.4 L/s was used in the first stage. This was increased to 2.1 L/s after 70 h, when the second stage started. The discharge was increased to 2.8 L/s after 140 h, when

the third stage started. The third stage and the whole experiment ended after 210 h.

Detailed replication of the geometry of a braided channel is impossible, both for physical and numerical models. Instead, parameters describing the braiding pattern can be used. Egozi and Ashmore (2009) measured the braiding intensity (BI) in the flume each hour of the experiment, in 13 cross sections. The average braiding intensity for all the cross sections was then computed and the values presented as a time series. The active braiding intensity (BI_A) was computed as the average number of active channels in the cross section. An active channel was defined as a channel with visible sediment transport, or particle movement. The total braiding intensity (BI_T), was defined as the number of channels with a finite water depth in a cross section. The active braiding intensity started at one in the first stage of the experiment and increased to 1.84 as an average value for the third and final stage. The total braiding intensity also started at one and increased to four at the end of the experiment.

3. Numerical model

The computer program used in the current study is called SSIIM (Sediment Simulation In Intakes with Multiblock option), and has been applied to a number of previous studies on 3D numerical modelling of sediment transport (Olsen, 1994; Olsen, 2003; Ruether and Olsen, 2007; Zinke et al., 2011; Olsen, 2017).

The numerical model solved the Navier-Stokes equations in three dimensions to find the water velocities. A fully 3D solver was used, where the vertical velocity was computed with the same algorithms as the two horizontal velocity components. A non-hydrostatic pressure could thereby be computed. The SIMPLE method was used to calculate the pressure, and the turbulence was computed by the k-epsilon model (Launder and Spalding, 1974). The numerical algorithms for computing the water velocities had previously been tested on a number of other cases, for example, in modelling local scour (Baranya et al., 2015) and a two-stage channel (Wilson et al., 2003).

The changes in the water surface elevations were computed by the IPDA method (Olsen, 2015). The algorithm uses an implicit method to compute the water elevation difference between cells using the pressure field found by the SIMPLE method. The downstream water level was kept fixed as a boundary condition, but the rest of the free surface would move according to the numerical solution procedure. An adaptive grid was used in the vertical direction, following the computed free surface.

The sediments were computed by a convection-diffusion equation for suspended sediments and bedload. The Engelund and Hansen (1967) formula was used to compute the pick-up rate of the particles and the sediment transport, q_s:

$$q_s = 0.05 \rho_s U^2 \sqrt{\frac{d_{50}}{g\left(\frac{\rho_s}{\rho}-1\right)}} \left[\frac{\tau}{g(\rho_s-\rho)d_{50}}\right]^{3/2} \qquad (3)$$

The depth-averaged velocity is denoted U, d_{50} is the average particle size, g is the acceleration of gravity, ρ is the density of water, ρ_s is the density of the sediments (2650 kg/m^3) and τ is the bed shear stress. The numerical model for computation of the water velocity in combination with sediment transport was previously tested by Haun et al. (2013). They computed suspended sediments concentrations in a hydropower reservoir and compared the results with field measurements.

The continuity equation for the sediments was used to compute the vertical elevation changes of the bed. Two grids were used: a 2D depth-averaged orthogonal grid that covered the whole flume geometry, both the wet and the dry areas. This grid was kept constant during the simulations. The cells were 4 cm in the longitudinal direction and 2.5 cm in the lateral direction. A coarser grid was also used, where the cells

were 5 cm in the longitudinal direction and 3 cm in the lateral direction. The fine 2D grid therefore had 450×120 cells and the coarse grid had 380×100 cells. The changes in the water and bed levels were computed in the 2D grid. These values were then used to generate an unstructured 3D grid, where the number of cells in the vertical direction was a function of the water depth. The regeneration of the grid for each time step meant that an adaptive 3D grid was used, where the total number of cells in the grid varied over time. The Navier-Stokes equations and the sediment transport were computed in the 3D grid.

Fig. 1 shows details of the grid in plan view (A) and a cross section (B). The plan view of the grid shows the 3D wetted area. The areas not covered with cells are dry. Also, note the change in the shape of the cells close to the banks. The rectangular shape can be modified somewhat to follow a complex geometry.

The cross section in Fig. 1 shows three branches of the braided system. The number of grid lines, n, in the vertical direction was computed from Eq. (4). The equation is based on the water depth, d, in the corners of a 2D cell:

$$\begin{aligned} &n = 0 \text{ if } d < d_{c1} \\ &n = 2 \text{ if } d_{c1} < d < d_{c2} \\ &n = n_{\max}\left(\frac{d}{d_{\max}}\right)^{0.7} \text{ if } d > d_{c2} \end{aligned} \qquad (4)$$

The values used in the current study were $n_{max} = 9$ and $d_{max} = 2$ cm. In the default computation, the values of d_{c1} and d_{c2} were 3 mm.

The values from Eq. (4) were applied to the four corners of each 2D grid cell. The number of cells generated in the vertical direction would be the maximum of these four values minus one. If the water depth was below the value of the d_{c1} parameter for all four corners of a 2D cell, no 3D cell would be generated. The 2D cell would thereby be dry in the next time step. The areas without cells in Fig. 1A are dry. Also, the part of the cross section in Fig. 1B without cells have dried up. This would be the area between the channels in the cross section.

Many studies of braided rivers using a 2D numerical model will use special algorithms to take lateral movements of the channels into account. Often, empirical formulas are used for the magnitude of the lateral migration. Steep banks at the outside of a bend of a river may collapse because of geotechnical failures. Several models exist for such processes, for example Ikeda et al. (1981) and Olsen and Haun (2018). In the current study, the banks were not very high, and the sediments did not have substantial cohesion. The lateral migration was therefore not computed explicitly by a specific formula. Instead, the migration of the channels was implicitly computed by the wetting/drying algorithm. Further details of the method are given by Olsen (2003).

The numerical model used a non-uniform sediment grain size distribution with 10 multiple fractions. This was similar to earlier work by Sun et al. (2015). The initial bed sediments were made up of 10% of each of the 10 sizes. The particle diameters were taken from the data of the laboratory experiment by Egozi and Ashmore (2009). Table 1 shows the details of the grain sizes, with particle diameters and initial grain size distribution.

The continuity algorithm for the bed elevation changes was used for each size as the erosion and deposition were computed, resulting in changes in the grain size distribution over time.

The bed roughness, k_s, was computed from the following formula (van Rijn, 1982):

$$k_s = 3d_{90} \qquad (5)$$

The parameter d_{90} is the grain size where 90% of the material is finer. The roughness was used in the wall laws solving the Navier-Stokes equations. The parameter affected the magnitude of the bed shear stress. In cells with erosion, the coarser size would dominate, causing a larger roughness. This would again increase the bed shear stress and the sediment transport capacity. Cells with deposition of the finest
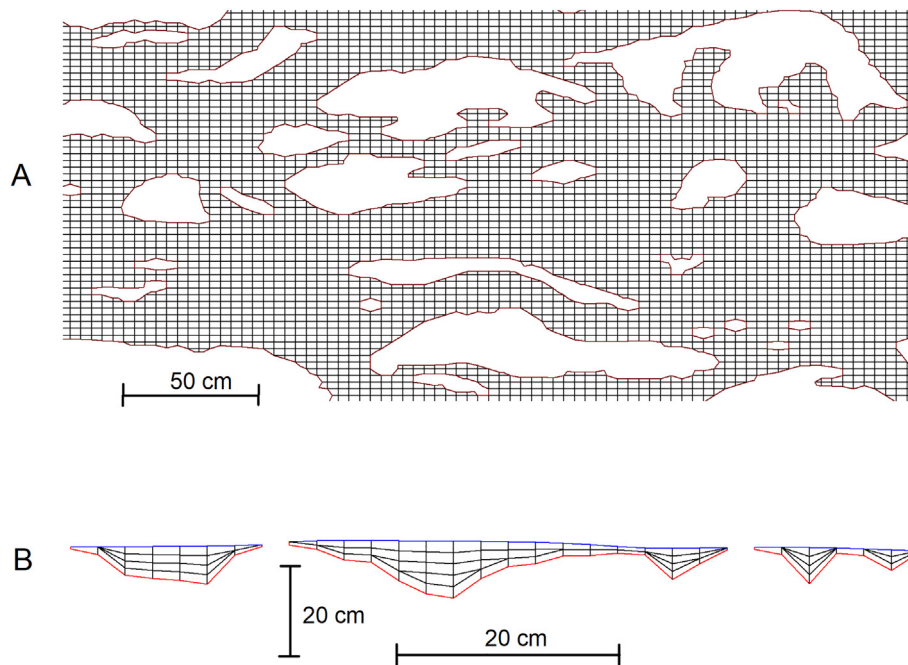
Fig. 1. A part of the grid seen in plan view (A) and in a cross-section (B).

fraction would have a lower roughness and again a lower shear stress. This would cause a reduced sediment transport capacity. These processes would only be possible to model with multiple sediment sizes. The variation of the roughness as a function of changes in the grain size distribution was found to be important by earlier studies (Vázquez-Tarrío et al., 2017).

The Navier-Stokes solver, sediment module and grid algorithms were all included in one program, so that each module had common access to all the necessary variables. Special functions to transfer variables from one module to another were therefore not needed.

A time step of 4 s was used in all the runs. With a total simulated time of 210 h, this meant that 189,000 time steps were used. The computational time for the 210 h of the physical experiment was five days on a PC with a 3.6 GHz i7 processor on the coarser grid. Eight days were needed for the fine grid.

4. Braided channel formation

The numerical model was used with input data from the initial geometry of the physical model study of Egozi and Ashmore (2009). The time series of inflowing water discharge from the physical model study was given to the numerical model. Recirculation of the sediments was computed by the numerical model, in that the sediment concentration at the upstream boundary was set equal to the outflow concentration. The resulting computed water depth is given in Fig. 2 for different

Table 1
Grain size distribution.

Size number	Diameter (mm)	Initial part in bed material (%)
1	4	10
2	3	10
3	2.1	10
4	1.7	10
5	1.3	10
6	1	10
7	0.75	10
8	0.55	10
9	0.45	10
10	0.2	10

times during the simulation. The figure shows that initial perturbations of the uniform flow field formed at the upstream end, spreading downstream. At 18 h, a wavy depth pattern had formed over the whole length of the flume. This pattern was also observed in laboratory models (Einstein and Shen, 1964) and the numerical modelling results of Zhang et al. (2020). The variation in depth increased over time, causing multiple channels to form in the initially 50 cm wide channel. The initial erosion/deposition process was similar to the formation of a meandering river (Olsen, 2003). In the current case, some channels started to show a non-symmetrical pattern at 31 h in Fig. 2. The braided channels then expanded in the lateral direction and formed more branches over time. The channels had different widths, often with one main channel and smaller side channels. This was also observed by Egozi and Ashmore (2009) in their physical model study. The channels formed and disappeared in a typical braided pattern.

One of the differences between a 3D and a 2D numerical model is the computation of the secondary currents. This parameter was believed to be important for the formation of a meandering and braided channel system. To study the effect of the secondary current in the 3D model, the vertical diffusion coefficient in the Navier-Stokes equations was multiplied with a factor five. The increase in the diffusion coefficient caused a stronger connection between the velocities at the bed and the surface. Thereby, the secondary current was reduced. The resulting braided channel evolution given in Fig. 3. Comparing Figs. 2 and 3, it is seen that the increase in the vertical diffusion coefficient produces less braiding. Fewer channels are seen in Fig. 3 than in Fig. 2.
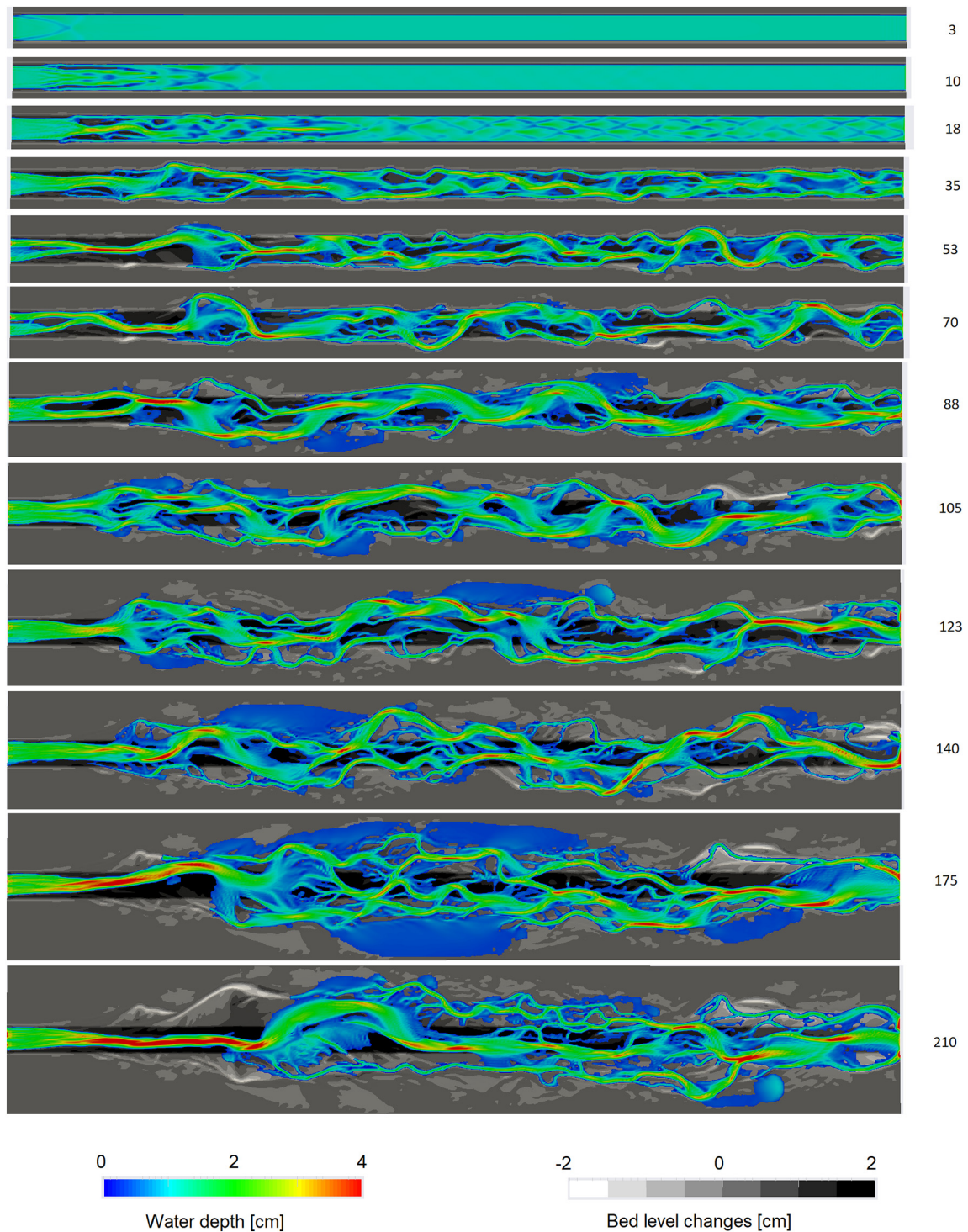
The avulsion processes are also more clearly seen. At 123 h, the most upstream bend to the left (upper) side is formed. At 140 h, a chute has formed and at 175 h the bend is dry. However, at 210 h, the water level in the bend has risen, so the previously dry bend is wet again.

One of the input parameters for the numerical model is the critical depth for the wetting/drying process. The default computation uses a d_{c1} value of 3 mm (Eq. (4)), which is 12% of the width of the cells for the fine grid. To investigate the importance of this parameter, a computation was done with a d_{c1} value of 2 mm instead. Additionally, the criteria for deciding if only one cell should be used over the depth (d_{c2} in Eq. (4)) was changed from 3 to 4 mm. This meant more 2D cells in the shallower areas. The results are shown in Fig. 4.

The first 18 h of the run seems to be similar for Figs. 2 and 4. The braiding process will have a random feature as also seen in a physical
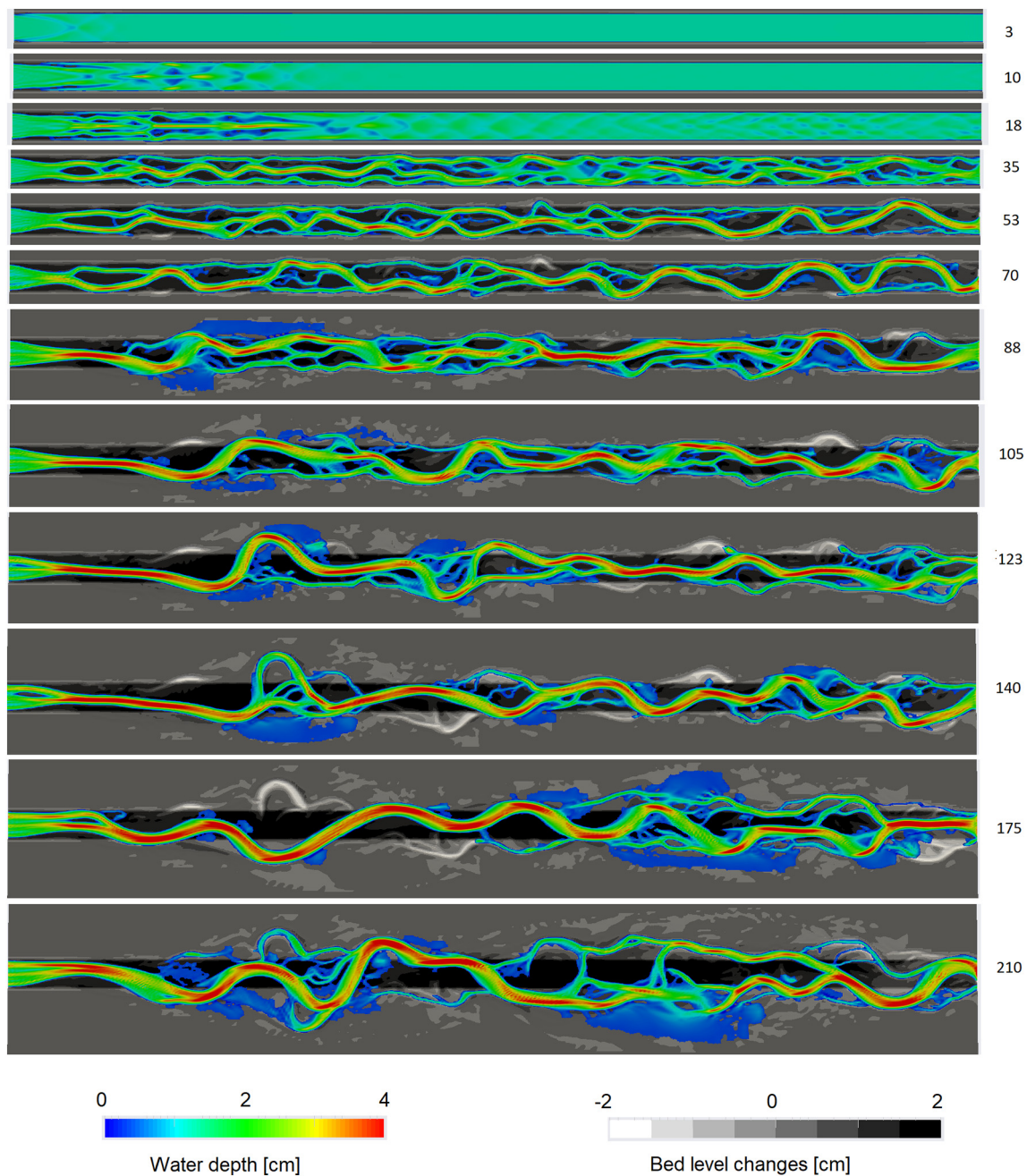
Fig. 2. Plan view of the channel with computed water depths for the default parameter configuration. The legends are depths and bed level changes in cm, and the numbers on the right are time in hours from the start. The water flow direction is from left to right. The length of the flume is 18 m. Colour animations of these results are given at http://pvv.org/~nilsol/cases/braided.

model. This means that small differences at one point can give large changes in the following braiding pattern. Comparing the results after 210 h for Figs. 2 and 4 shows a different pattern. But it is difficult to say if more or less braided channels have been formed.

Another parameter that is often very important in CFD modelling is the grid size. The current study used two grids: a coarse and a fine. Although the difference in size was not large, a comparison of the results from the two grids can be interesting. The first three

computations were done with the fine grid (Figs. 2–4). Fig. 5 shows the braided channel evolution using the coarser grid with the same parameters as used for the results in Fig. 2. Looking at 18 h in Fig. 5, the depth pattern is less pronounced than in Fig. 2. This is because of the coarser grid. Comparing Figs. 2 and 5 after 18 h is difficult because of the random nature of the braided system. However, the number of parallel channels and the braiding intensity seems similar.

Fig. 3. Plan view of computed water depths with an increase in the vertical diffusion coefficient with a factor 5. The legends are depths and bed level changes, and the numbers on the right are time in hours from the start. The water flow direction is from left to right.

The basis of the numerical modelling of sediment transport is the sediment transport capacity, given by a transport formula. The Engelund-Hansen (1967) formula was used in the previously described results, but it was also interesting to see what other formulas produced. The default computation was therefore repeated with two alternative sediment transport formulas: The bedload formula of van Rijn (1984) and the Meyer-Peter and Mueller (1948) formula, called MPM from this point forward. These two formulas were also used in the modelling of a braided river by Lotsari et al. (2014). Sun et al. (2015) also used the van Rijn formula. The result using the van Rijn formula is given in Fig. 6. The other parameters used for this computation were similar to the default computation, which is shown in Fig. 2.

Fig. 6 shows a different braiding pattern that the results from the Engelund-Hansen formula (Fig. 2). Lateral erosion of the initially

straight channel continues, forming a meandering pattern. This pattern grows laterally over time, similar to the previous results. However, there is much less braiding. At 105 h, one of the larger meander bends was cut off, and during this process multiple channels existed. Also, at 175 h, one of the bends has two channels. The main part of the geometry, however, only has one channel.

Another sediment transport formula that has been used over many years is the MPM formula. The default computation was also repeated using this approach. The results are given in Fig. 7.

The results in Fig. 7 are more similar to the planform of Fig. 6 than Fig. 2. The MPM formula gives fewer braiding channels than the Engelund-Hansen formula. The initial channel expands more slowly in the lateral direction after 35 h, compared with both the Engelund-Hansen and the van Rijn formula. From 105 h, meander cut-offs are seen in steps, producing multiple braiding channels. However, the
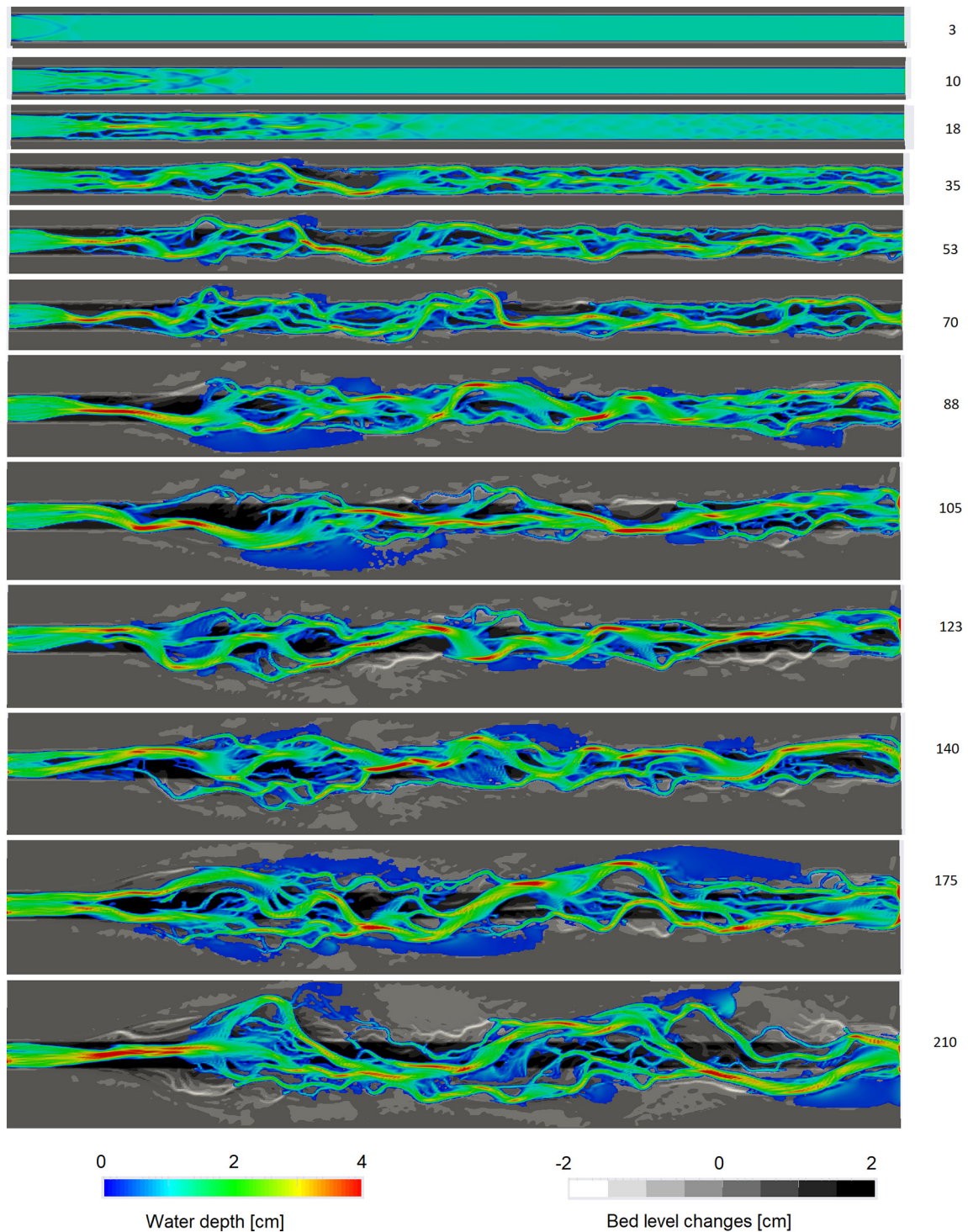
Fig. 4. Plan view of computed water depths with modified depth criteria for the wetting/drying of cells. The legends are depths and bed level changes in cm, and the numbers on the right are time in hours from the start. The water flow direction is from left to right.

main channel pattern is more similar to a meandering river than a braided system.

5. Braiding intensity

Because the evolution of the braided channel has a random component, it is difficult to compare measured and computed braided channel patterns directly at one particular time from a plan view as shown in Figs. 2–7. Lotsari et al. (2014) attempted this with geometry data from echo soundings in the Tana River in Norway, but the computed and measured braiding patterns were not similar.

The proposed solution to this problem is the previously described parameter braiding intensity (*BI*) (Egozi and Ashmore, 2009). This parameter was also computed in the numerical model. All cross sections downstream of the first four meters were used and averaged. The computation was done for each 400 s. The total number of channels was
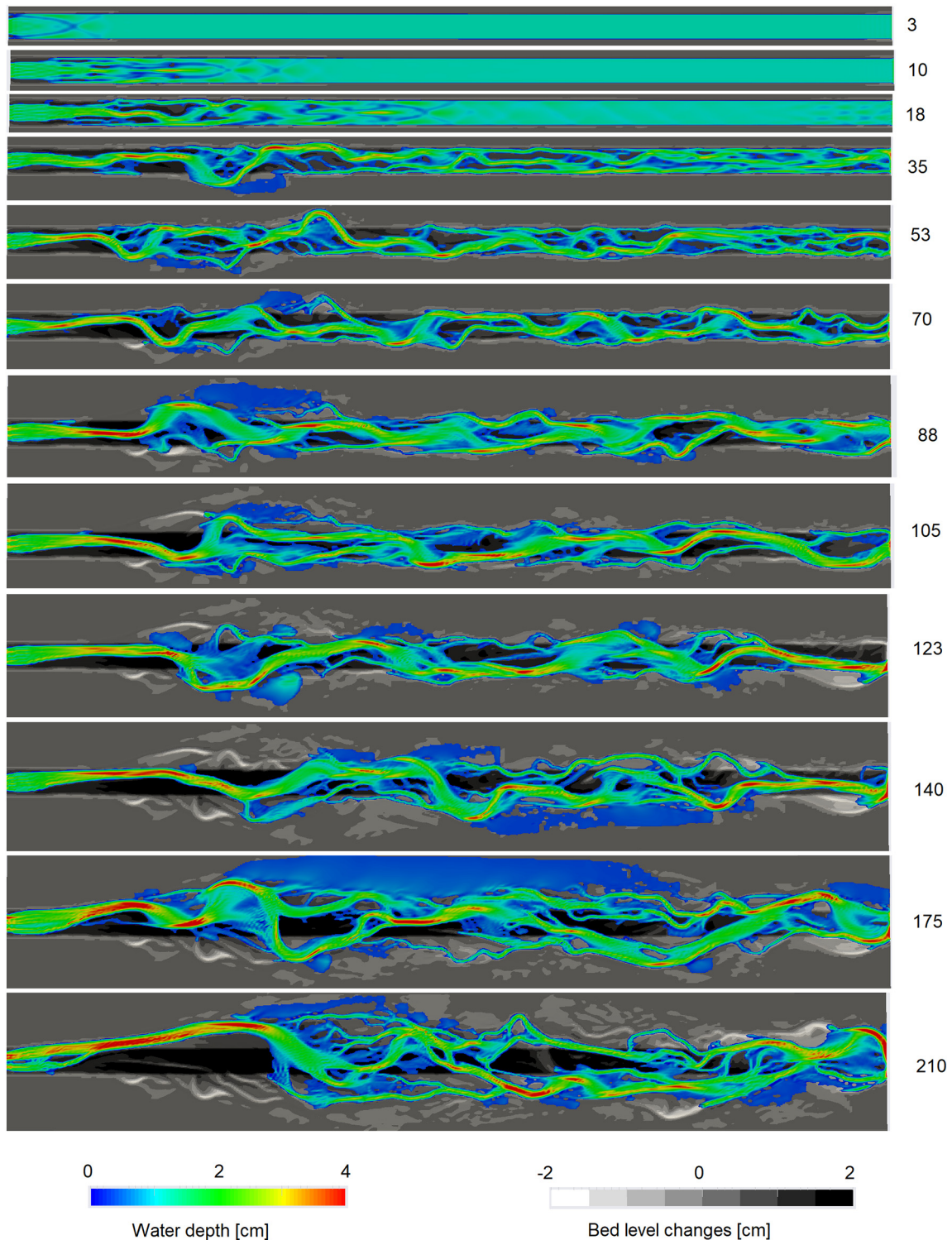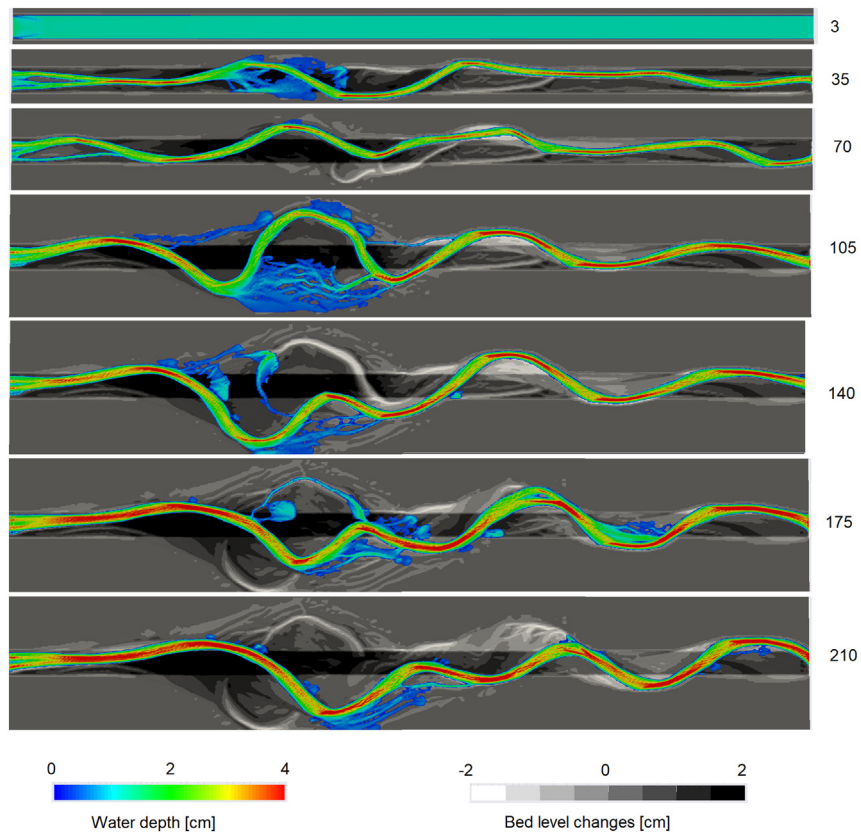
Fig. 5. Plan view of computed water depths with the coarser grid. The legends are depths and bed level changes, and the numbers on the right are time in hours from the start. The water flow direction is from left to right.

computed from the cells that had a finite water depth. For BI_A, criteria for determination of sediment movement was needed. Using Shields (1936) curve for the d_{75} of the grain size distribution gave a critical shear stress of 1.0 Pa. This value was used in defining a cross section with active sediment transport. For the fine grid, at least four neighbouring cells in a cross section had to have a shear stress exceeding this value to be counted in the active braiding intensity. Only three cells were used for the coarse grid. Because the cell size in the transverse

direction was 2.5 cm for the fine grid, this meant that the shear stress had to exceed the critical value over a channel width of 10 cm to be defined as an active channel. For the coarse grid, this critical width was 9 cm.

The braiding intensities provided a numerical value to compare the results from the physical and numerical models (Sun et al., 2015). Fig. 8 shows the resulting computed active braiding intensity for the default configuration and the test where the secondary current was

Fig. 6. Plan view of channel evolution using the van Rijn bedload formula. The legends are depths and bed level changes and the numbers on the right are time in hours from the star. The flow direction is from left to right.
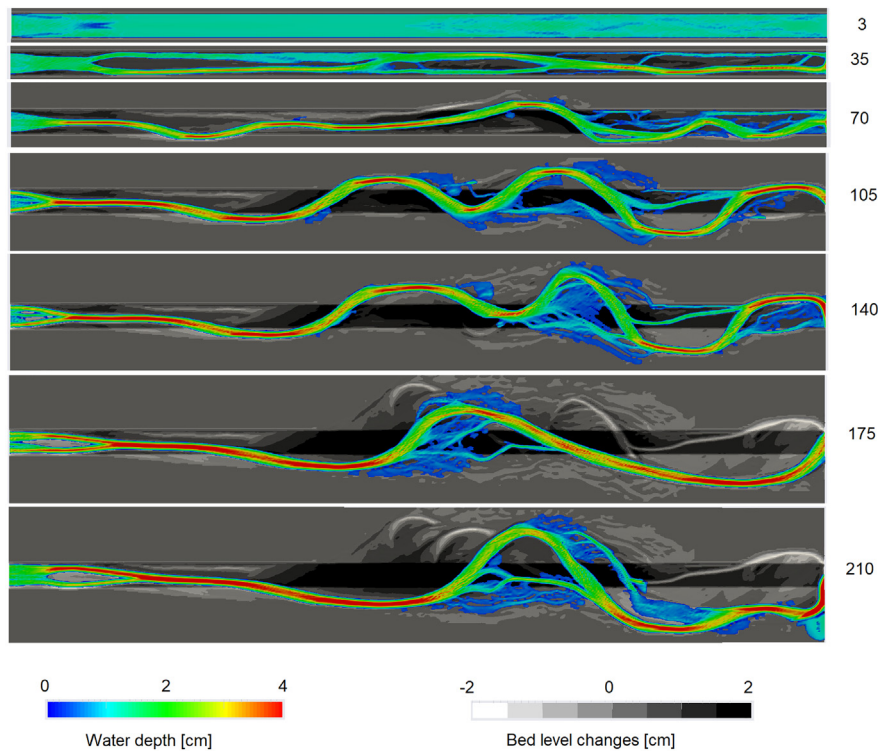
Fig. 7. Plan view of channel evolution using the MPM formula. The legends are depths and bed level changes and the numbers on the right are time in hours from the star. The flow direction is from left to right.
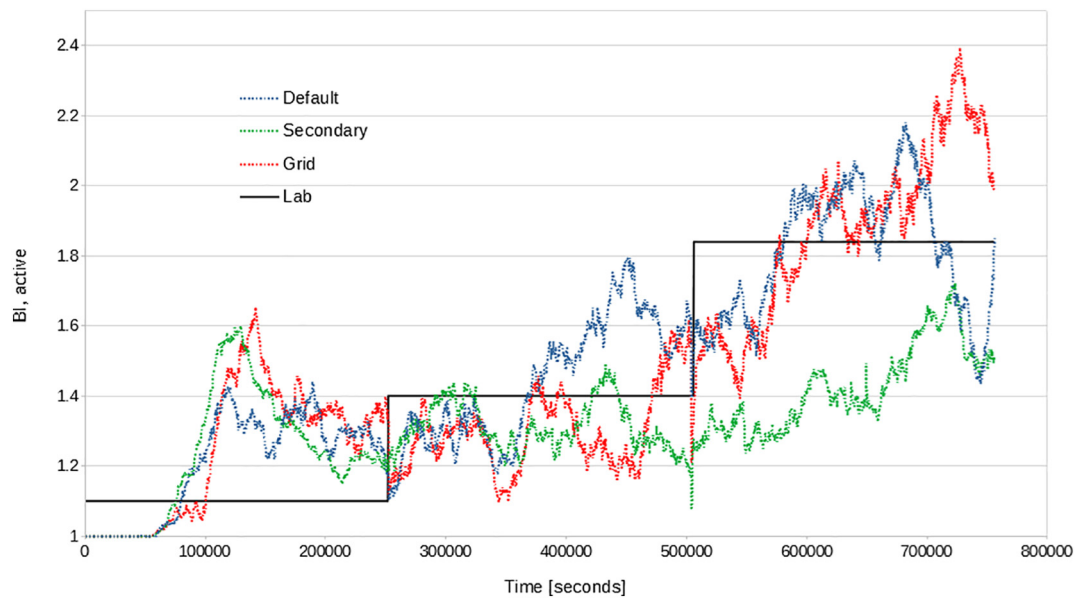
Fig. 8. Time series of computed Active Braiding Intensity (BI_A). Average values over each time period are shown from the laboratory experiment.

damped by increasing the vertical diffusion. It also shows the results from the coarser grid. The average BI_A values for each of the three discharges are also shown from the laboratory study.

Fig. 8 shows that the BI_A value starts at one and increases over time, with considerable fluctuations. This was also observed in the results from the physical study. The increase of the BI_A value is less pronounced for the computation with the dampened secondary current, particularly in the last discharge period. This is similar to what was observed in Fig. 3.

Comparing the results of the physical model study with the computed values from the numerical model can also be done in a table using time-averaged values of BI_A. Table 2 shows the computed and measured BI_A values for the different model runs during the three discharge periods.

A systematic difference between the computed and measured active braiding intensity is observed in the first time period. The computed BI_A value is around 1.2, while the measured laboratory value is around 1.1. This is a 10% difference. Figs. 2–5 show that more than one channel emerge at 35 h. The numerical model was started with a wet channel that had perfectly uniform flow from time zero. This was probably not possible in a physical model. The difference in initial boundary conditions may have affected the formation in the special depth-pattern shown after 18 h in Figs. 2–5. This caused a several parallel channels to form, leading to the high BI_A value in the first period.

The results from the four different computations using the Engelund-Hansen formula presented in Table 1 all show that the BI_A increases up to around 1.8 at the end of the simulation in Period 3. The exception is the run with the reduced secondary current, which only shows a BI_A value of 1.44. This is in line with observations from Fig. 3

Table 2
Active Braiding Intensities (BI_A) for different runs and periods.

Model	Period 1	Period 2	Period 3
Laboratory	1.1	1.4	1.84
Default computation	1.20	1.44	1.81
Secondary current	1.22	1.31	1.42
Grid parameters	1.14	1.31	1.78
Coarser grid	1.24	1.30	1.87
Van Rijn formula	1.09	1.04	1.10
MPM formula	1.18	1.16	1.14

that the reduction of the secondary currents causes less braiding. The BI_A values are also smaller when using the van Rijn and the MPM formula, which corresponts well with the observations in Fig. 6 and 7.

6. Chute cutoff

The channels in a braided river system will bifurcate at several locations. Ferguson (1993) described chute cutoffs as local avulsions. Slingerland and Smith (2004) described avulsion as a process where the water flow diverts from the main channel into a new course on the floodplain. A full avulsion would leave the original channel dry, whereas a partial avulsion would mean that water would flow in both channels. A braided system with multiple parallel channels would imply that avulsions had to have taken place.

Once the numerical model is verified to replicate the braided system formation, it can also be used to give insights into the avulsion processes (Yang et al., 2018). Important characteristics are erosion, sediment transport, secondary currents and changes in water surface elevations. The secondary current occurs in bends where the high-momentum water close to the surface moves more towards the outside of the bend. The water at the bed will then be forced more to the inside of the bend. The 3D grid used in the current study had multiple cells located directly above each other (Fig. 1B). In a plan view, the velocity vectors in the surface cell and in the bed cell below will then start from the same point: the centre of the two cells. These two vectors are shown in Fig. 9, where the circle marks the cell centre. The angle between these two vectors is denoted a in the figure. This is the secondary current angle.

Because the sediments move mostly as bedload, the particles will move in the direction of the velocity vector close to the bed towards the inside of a bend. Erosion will normally take place at the outside of the curve. The process will lead to a lateral movement of the channel.

The bend flow will also produce a higher water surface elevation at the outside of the curve because of the centrifugal force. This may cause the flow to spill over the bank. If an already existing channel is located at the outside of the curve, the water may follow this channel. Slingerland and Smith (2004) classified this process as avulsion by annexation. The water close to the surface at the outside of the curve will have a higher velocity, causing erosion at the entrance of the new channel. The new channel may also form in a curve, with deposition
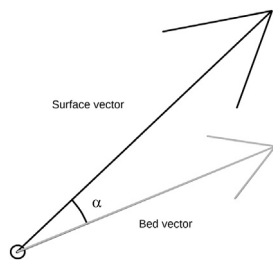
Fig. 9. Definition of the secondary current angle, a, from the velocity vectors at the surface and at the bed. The vectors are shown in plan view.

on the inside of the bend. This may cause most of the bedload to move towards the old channel. The decreasing water discharge in the old channel can cause the bed levels here to increase. The water surface elevation will also be lower at the inside of the curve, which now is the old channel. The reduced water level and increased bed level at the old channel will decrease its capacity to transport water. More of the water will therefore enter the new channel.

The braided channel formation presented earlier includes a number of abrupt changes in the channel geometry. A selection has been made to focus on a chute cutoff taking place in the run with the increase in the vertical diffusion with a factor of five (Fig. 3). The particular bend studied in more detail is shown at the downstream part of the system in Fig. 3. During the time period from 180 to 210 h, there is a meander bend that is being cut off by formation of a new chute. An enlargement of the bend is shown in Fig. 10, giving more details. Also, images are shown for more time steps to better understand the temporal evolution.

The process starts with the bend shown at 180 h. Because of sediment transport and the secondary current, the bend moves downstream and increases in amplitude. At 190 h, the water spills over the left bank of the first bend, which initiates the chute. Erosion occurs in the chute, which deepens as shown at 200 h. At 210 h, the new channel

has formed where the chute started, and the old channel has partly dried up. This is the classical avulsion of a meander bend.

An interesting question that arises is whether the numerical model can shed light on more details of this process? Parameters such as the secondary currents and water elevations are not trivial to measure in detail in a physical model with a changing geometry. Fig. 11 shows the same bend as in Fig. 10 at 190 h, but with four different parameters: water depth, water velocity, water level and secondary current strength. The water depth is large in the main channel, although the water level has increased over the left overbank of the main curve. The velocity also follows the main channel, meaning that there is no sediment transport overbank. Fig. 11C shows the water elevation. The white arrow points to the location where the chute starts. This is at the outside of the first upstream bend. The centrifugal force causes the water level to be higher at the outside of the bend. The upstream bend therefore creates an elevated water level where the chute starts. A rise in water level in the main channel was also found by van Dijk et al. (2014) to be important in the formation of the chute.

Fig. 11D shows the secondary currents in the bends. The black/red areas indicate strong secondary currents with a bed vector component to the right in the flow direction. Erosion of sediments from the outside of the bend follows. This is exactly what occurs at the location where the chute starts to form. The erosion causes the bed level in the start of the chute to be lowered. Together with the heightened water level caused by the centrifugal force, this increases the water depth at the upstream part of the chute. This is important in the avulsion process as a given water depth is required to transport sediments. Another important effect of the secondary current is that the main bedload is directed towards the inside of the curve, which is away from the chute inlet. Water with less sediment will therefore enter the chute, facilitating bed erosion and deepening of the chute.

Fig. 12 shows the channel bends at 195 h. The water depth in the chute has increased together with the water velocity. The water level still has a high value where the chute starts (Fig. 12C). This is pointed to with the white arrow. The discrete shades in the figure makes it possible to observe contour lines of water elevations. Note that the contour lines are more narrowly spaced in the direction of the chute than in the
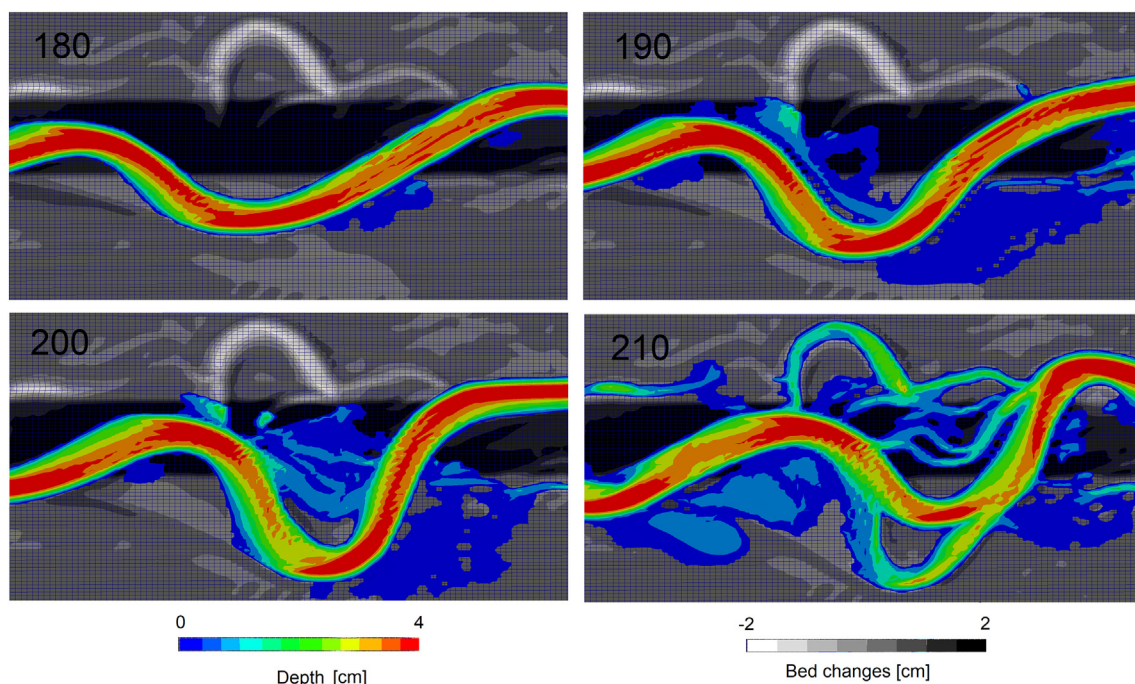

Fig. 10. Computed water depths during a local avulsion. The numbers are times in hours. The water flow direction is from left to right.
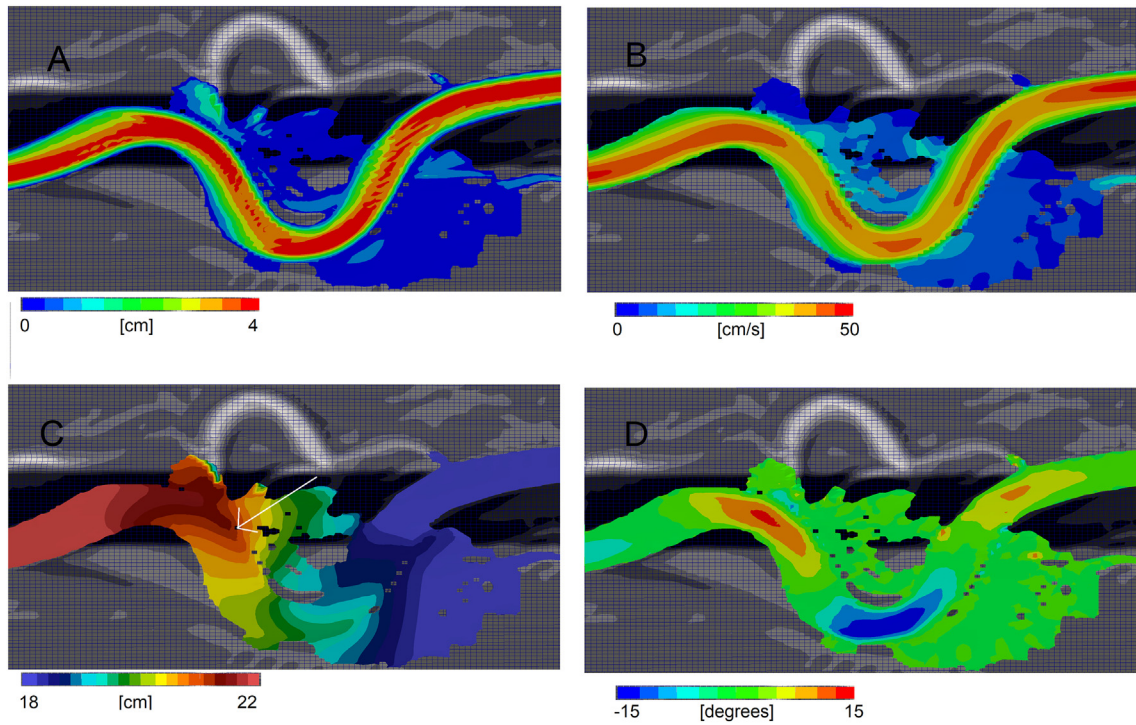
Fig. 11. Plan view of a channel section at 190 h for the computation with reduced secondary currents. A: water depth, B: water velocity, C: water level, D: secondary current. The flow direction is from left to right.

main channel. The water will flow a shorter distance in the chute than in the bend. The water surface slope will therefore be steeper in the chute than in the channel. The bed shear stress in a channel with uniform flow is proportional to the water surface slope. The shorter flow distance through the chute will therefore cause an increased bed shear stress and erosion.

Fig. 12D shows the secondary current at 195 h. The secondary current is still strong in front of the chute, causing clearer water to enter it. The sediments are directed towards the old channel. As the water discharge through the chute increases, less water will flow through the original bend. Comparing Figs. 11B and 12B shows that the velocity has decreased slightly. The lower velocity causes the sediment transport
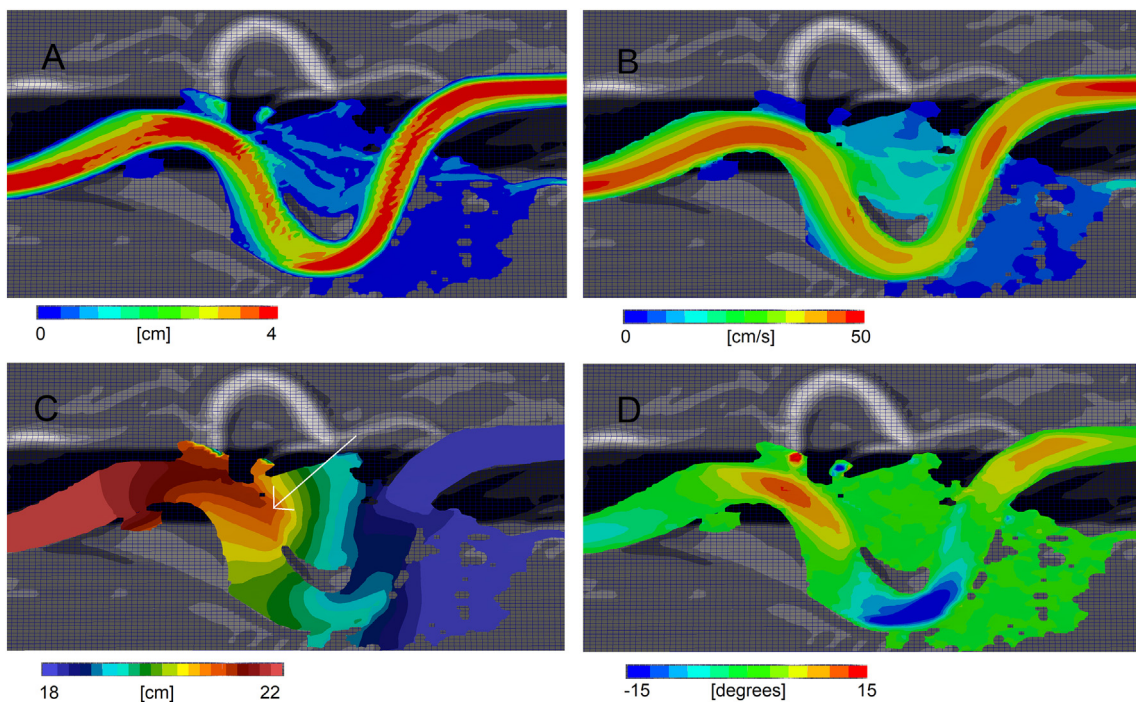
Fig. 12. Plan view of a channel section at 195 h for the computation with reduced secondary currents. A: water depth, B: water velocity, C: water level, D: secondary current. The flow direction is from left to right.

capacity to decrease. The sediments that are pushed into the old bend by the secondary current will therefore have a tendency to be deposited. This causes the water depth in the original channel to decrease, pushing more water into the chute.

Van Dijk et al. (2014) stated that sediment partitioning was important in the formation of the chute cutoff. The current study shows that the secondary current, or the helical flow, will move sediments to one side of the channel. At a bifurcation point, this leads to more sediments flowing into one branch than the other. When the sediments are moved away from the chute, then they will move into the original channel. The higher sediment inflow combined with the lower water velocity and sediment transport capacity will lead to sediment deposition in the original channel. This process will cause more water to flow into the chute and accelerate the cutoff.

7. Discussion

A braided channel system will evolve with a random component. It is therefore not possible to exactly replicate a laboratory model study of a braided channel in all details. The currently used numerical model uses an OpenMP parallelization algorithm where the different cores in the computer will handle separate parts of the grid. After each core is finished, the results are sent to the other cores, which use the incoming values as boundary conditions. Using standard solvers, this will give somewhat different results depending on which core finishes the computation first. A standard solver will therefore give a slightly different result if the same computation is done twice. This will not affect the results in a significant way for most CFD computations, but for a braided

system only a small perturbation will increase to produce different geometrical patterns. This means that running the same braided computation multiple times will lead to different braiding patterns (Figs. 2–7), different time series (Fig. 8) and also different BI_A values (Table 2), even if the identical initial and boundary conditions are used. In the current study, a special solver is made so that the parallelization problem is avoided and exactly the same result is produced if a run is done twice. However, the results must still be viewed as one solution of possibly many for the same boundary condition. A similar random component also exists in a laboratory study. Two laboratory runs with a braided river will also not produce exactly the same geometrical pattern. The computed BI_A values in Table 2 will therefore have a fair amount of uncertainty.

The sediment transport formula seems to have a significant effect on the braided pattern. The current study shows that the formula by Engelund-Hansen gives higher braiding intensities than the van Rijn or MPM formulas. A possible reason is that the Engelund-Hansen formula gives a higher sediment transport capacity than the other formulas. The Engelund-Hansen formula also gives a finite sediment transport if the bed shear stress is above the critical value given by Shields (1936). The other two formulas will give zero sediment transport capacity in such cases. The sensitivity of the results to the sediment transport formula was also found by Lotsari et al. (2014), modelling the braided Tana River in Norway. Both the van Rijn and the MPM formula gave reasonable results for the bed elevation changes. The formula by van Rijn was found to give a more stable result.

The current study focuses on secondary currents as one of the main parameters affecting braided channel evolution. A damping factor is
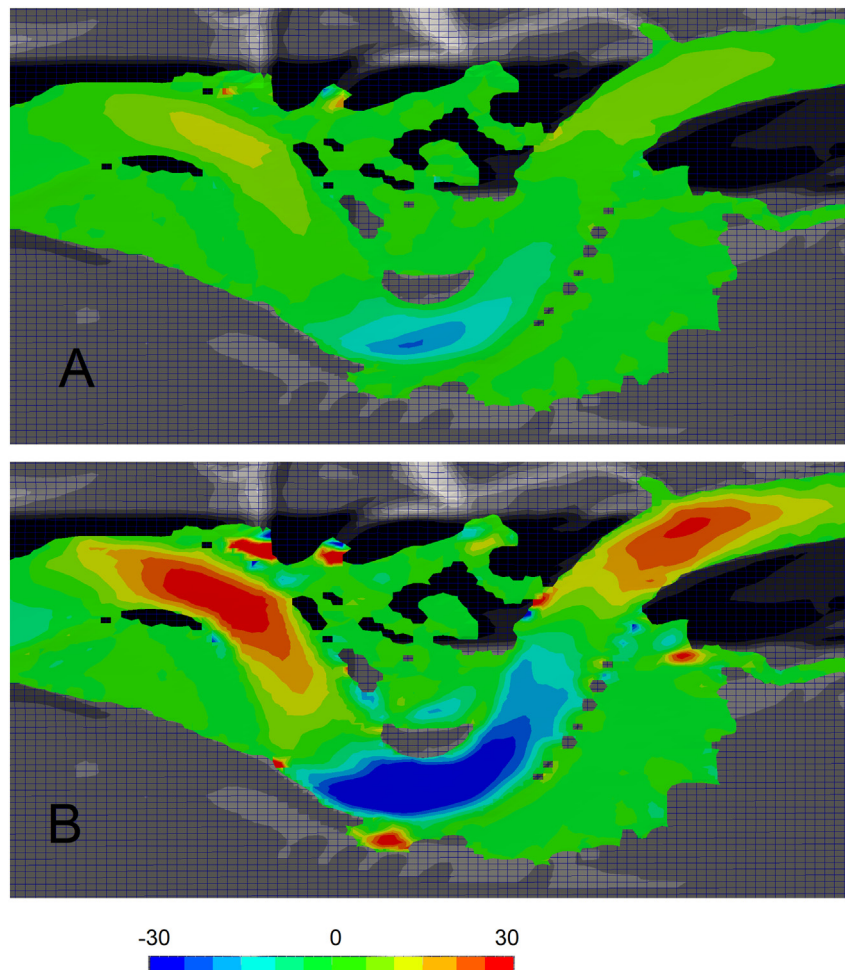

Fig. 13. Secondary currents in the bend from Fig. 3, with an increase in the eddy-viscosity (A) and no increase (B).

introduced for the secondary current by increasing the vertical diffusion. The increase in the vertical eddy-viscosity should in theory give less secondary currents in bends, as it increases the connection between the velocity vectors at the bed and the surface. Comparing Figs. 2 and 3 shows a substantial difference in the braiding intensity. But are we sure that this is caused by the secondary currents? To investigate this question, the computation with an increase in the vertical eddy-viscosity (Fig. 3) was stopped at 190 h and the bed and water surface was frozen. The water flow field was then recomputed without any increase in the vertical eddy-viscosity. The resulting secondary current angles for the two cases are shown in Fig. 13. The increase in the vertical eddy-viscosity with a factor of five gives secondary angles that are less than half of the original values. This shows that the increase in the vertical eddy-viscosity affects the secondary currents substantially.

The next question regarding the secondary current damping is if this actually takes place in nature? Photos from the physical model study (Egozi and Ashmore, 2009) show ripples on the bed. Such bedforms are often seen in physical models. Also, in natural rivers bedforms such as dunes and antidunes occur. Ripples, dunes and antidunes will introduce an extra vertical velocity component in the main flow because of their geometry. A convective transport of momentum and turbulence will take place in the vertical direction, which can reduce the secondary currents. Also, there is often a variation of the water depth over bedforms, which can introduce extra turbulence. Bedforms can be modelled numerically (Olsen, 2017), but usually around 30–50 cells are required for each ripple/dune to be modelled with a proper spatial resolution. In the current study, the ripples have dimensions similar to the size of one grid cell. The flow field over each individual ripple can then not be modelled directly in the CFD model because of the coarse grid. The solution chosen in the current study is to increase the diffusive term in the Navier-Stokes equations. It is therefore possible that the physically most correct results may not be what is seen in Fig. 2 as the default computation. Results closer to what is shown in Fig. 3 may be more in line with the processes in the physical model.

Another question related to avulsions is whether they are only formed during high discharges? This seems to be the case for many large floods. Hooke (2004) investigated multiple avulsions that took place in the River Bollin in the UK during floods in 2000–2001. A flood will cause an increase in the water velocity and sediment transport capacity of a river, increasing bank erosion and the possibility for geometrical changes. The current study shows that braiding and local avulsions also occur during constant water discharges. The two increases in the water discharge during the experiment did cause a rise in the value of the braiding intensity. However, the avulsion described in the previous section took place during a constant water discharge.

8. Conclusions

A 3D numerical model has been used to model the formation of a braiding channel. Computed time series of active braiding intensities compare reasonably well with observations from the laboratory experiment. The grid size and the critical depth for wetting/drying were tested in the current study. Both parameters had some effects on the results, but main features of the braiding patterns were not substantially changed. An important function for the evolution of the braided channel system was the sediment transport capacity. The Engelund-Hansen formula gave a higher braiding intensity than the formula by van Rijn or Meyer-Peter and Müller. The latter two formulas gave a planform more similar to a meandering river. Further studies with improved sediment transport formulas are a topic for future research.

The numerical model also showed details of a local avulsion process: how a chute is formed and how it is affected by the water depth, water surface location, water velocity and secondary current change. The changes in the water surface elevation were shown to be important during the avulsion. The water level would increase at the outside of the bend because of centrifugal forces at the location of the chute entrance.

Therefore, the water depth in the chute would increase, causing higher bed shear stress and erosion in the chute. The secondary current was also shown to be important, as it pushes the bedload away from the chute and into the main channel. In so doing, clearer water enters the chute, causing erosion and an expansion of the new channel. At the same time, the bedload is directed towards the old channel where the water discharge is reduced. The process promotes clogging of the old channel, which can lead to a complete avulsion. The fully 3D approach of the numerical model is able to predict the secondary current directly, instead of relying on empirical formulas, which is required in 2D models.

In a 3D model, the secondary currents could be controlled by varying the vertical turbulent diffusion coefficient in the Navier-Stokes equations. The increased diffusion would cause the bed and surface velocity vectors to be closer to each other in magnitude and direction. The physical reason for an increase in the vertical turbulence would be bedforms as dunes and antidunes, causing an increase in the vertical velocities over the water depth. This process is also a topic for future research.

Declaration of competing interest

The author declares that he has no known competing financial interests or personal relationships that could have appeared to influence the work reported in this paper.

References

Baranya, S., Olsen, N.R.B., Jozsa, J., 2015. Flow analysis of a river confluence with field measurements and RANS model with nested grid approach. River Res. Appl. 31 (1), 28–41. https://doi.org/10.1002/rra.2718.

Baranya, S., Fleit, G., Josza, J., Szaloky, Z., Toth, B., Czegledi, I., Eros, T., 2018. Habitat mapping of riverine fish by means of hydromorphological tools. Ecohydrology 11, 1–13. https://doi.org/10.1002/eco.2009.

Bertoldi, W., Welber, M., Mai, L., Zanella, S., Comiti, F., 2014. A flume experiment on wood storage and remobilization in braided river systems. Earth Surf. Process. Landf. 39, 804–813. https://doi.org/10.1002/esp.3537.

van Dijk, W.M., Schuurman, F., van de Lageweg, W.I., Kleinhans, M.G., 2014. Bifurcation instability and chute cutoff development in meandering gravel-bed rivers. Geomorphology 213, 277–291. https://doi.org/10.1016/j.geomorph.2014.01.018.

Egozi, R., Ashmore, P., 2009. Experimental analysis of braided channel pattern response to increased discharge. J. Geophys. Res. Earth Surf. 114, F02012. https://doi.org/10.1029/2008JF001099.

Einstein, H.A., Shen, H.W., 1964. A study on meandering in straight alluvial channels. J. Geophys. Res. 69 (24), 5239–5247.

Engelund, F., Hansen, E., 1967. A Monograph on Sediment Transport in Alluvial Streams. Teknisk Forlag, Copenhagen, Denmark.

Engelund, F., Skovgaard, O., 1973. On the order of meandering and braiding in alluvial streams. J. Fluid Mech. 57 (2), 289–302.

Ettema, R., Armstrong, D.L., Thornton, C.I., Huges, S.A., Abt, S.R., 2016. Hydraulic modelling of braided channels self-formed in an alluvial plain. Proceedings of RiverFlow 2016, New Orleans. ISBN: 978-1-138-02913-2.

Ferguson, R.I., 1993. Understanding braiding processes in gravel-bed rivers: progress and unresolved problems. In: Best, J.L., Bristow, C.S. (Eds.), Braided Rivers. Geological Society, London, pp. 73–87.

Fischer-Antze, T., Olsen, N.R.B., Gutknecht, D., 2008. Three-dimensional CFD modeling of morphological bed changes in the Danube River. Water Resour. Res. 44 (9), W09422. https://doi.org/10.1029/2007WR006402.

Haun, S., Olsen, N.R.B., 2012. Three-dimensional numerical modelling of reservoir flushing in a prototype scale. Int. J. River Basin Manag. 10 (4), 341–349. https://doi.org/10.1080/15715124.2012.736388.

Haun, S., Kjærås, H., Løvfall, S., Olsen, N.R.B., 2013. Three-dimensional measurements and numerical modelling of suspended sediments in a hydropower reservoir. J. Hydrol. 479 (4), 180–188. https://doi.org/10.1016/j.jhydrol.2012.11.060.

Hooke, J.M., 2004. Cutoffs galore!: occurrence and causes of multiple cutoffs on a meandering river. Geomorphology 61, 225–238. https://doi.org/10.1016/j.geomorph.2003.12.006.

Ikeda, S., Parker, G., Sawai, K., 1981. Bend theory of river meanders. Part 1. Linear development. J. Fluid Mech. 112, 363–377.

Jang, C.-L., Shimizu, Y., 2005. Numerical simulation of relatively wide, shallow channels with erodible banks. J. Hydraul. Eng. 131 (7), 565–575. https://doi.org/10.1061/(ASCE)0733-9429(2005)131:7(565).

Javernick, L., Hicks, D.M., Measures, R., Caruso, B., Brasington, J., 2016. Numerical modelling of braided rivers with structure from motion-derived terrain models. River Res. Appl. 32, 1071–1081.

Khosronejad, A., Kang, S., Flora, K., 2019. Fully coupled free-surface flow and sediment transport modelling of flash floods in a desert stream in the Mojave Desert, California. Hydrol. Process. 33, 2772–2791. https://doi.org/10.1002/hyp.13527.

Kim, J.S., Baek, D., Park, I., 2020. Evaluating the impact of turbulence closure models on solute transport simulations in meandering open channels. Appl. Sci. 10, 2769. https://doi.org/10.3390/app10082769.

Langendoen, E.J., Mendoza, A., Abad, J.D., Tassi, P., Wang, D., Ata, R., Abderrezzak, K., Hervouet, J.-M., 2016. Improved numerical modeling of morphodynamics of rivers with steep banks. Adv. Water Resour. 94. https://doi.org/10.1016/j.advwatres.2015.04.002.

Launder, B.E., Spalding, D.B., 1974. The numerical computation of turbulent flows. Comput. Methods Appl. Mech. Eng. 3 (2), 269–289. https://doi.org/10.1016/0045-7825(74)90029-2.

Li, S.S., Millar, R.G., 2011. A two-dimensional morphodynamic model of gravel-bed river with floodplain vegetation. Earth Surf. Process. Landf. 36, 190–202. https://doi.org/10.1002/esp.2033.

Liedermann, M., Tritthart, M., Habersack, H., 2013. Particle path characteristics at the large gravel-bed river Danube: results from a tracer study and numerical modelling. Earth Surf. Process. Landf. 38, 512–522. https://doi.org/10.1002/esp.3338.

Lotsari, E., Wainwright, D., Corner, G.D., Alho, P., Käyhkö, J., 2014. Surveyed and modelled one-year morphodynamics in the braided lower Tana River. Hydrol. Process. 28, 2685–2716. https://doi.org/10.1002/hyp.9750.

Meyer-Peter, E., Mueller, R., 1948. Formulas for bed-load transport. IAHR 2nd Meeting Stockholm, Sweden, pp. 39–64.

Olsen, N.R.B., 1994. SSIIM - A three-dimensional numerical model for simulation of water and sediment flow, HYDROSOFT-94, Porto Carras Greece.

Olsen, N.R.B., 2003. 3D CFD modeling of a self-forming meandering channel. J. Hydraul. Eng. 5, 366–372. https://doi.org/10.1061/(ASCE)0733-9429(2003)129:5(366).

Olsen, N.R.B., 2015. Four free surface algorithms for the 3D Navier-Stokes equations. J. Hydroinf. 17 (6), 845–856. https://doi.org/10.2166/hydro.2015.012.

Olsen, N.R.B., 2017. Numerical modelling of downstream migrating antidunes. Earth Surf. Process. Landf. 42, 2393–2401. https://doi.org/10.1002/esp.4193.

Olsen, N.R.B., Haun, S., 2018. Numerical modelling of bank failures during reservoir draw-down. RiverFlow 2018, Lyon, France https://doi.org/10.1051/e3sconf/20184003001.

Parsapour-Moghaddam, P., Rennie, C., 2017. Hydrostatic versus nonhydrostatic hydrodynamic modelling of secondary flow in a tortuously meandering river: application of Delft3D. River Res. Appl. 33, 1400–1410. https://doi.org/10.1002/rra.3214.

Randle, T.J., Bountry, J.A., Ritchie, A., Wille, K., 2015. Large-scale dam removal on the Elwha River, Washington, USA: erosion of reservoir sediment. Geomorphology 246, 687–708. https://doi.org/10.1016/j.geomorph.2014.12.045.

van Rijn, L.C., 1982. Equivalent roughness of alluvial bed. J. Hydraul. Eng. 108 (10), 1215–1218.

van Rijn, L.C., 1984. Sediment transport, part 1, bed load transport. J. Hydraul. Eng. 110 (10), 1431–1456. https://doi.org/10.1061/(ASCE)0733-9429(1984)110:10(1431).

Rousseau, Y.Y., Biron, P.M., Van de Wiel, M.J., 2016. Sensitivity of simulated flow fields and bathymetries in meandering channels to the choice of a morphodynamic model. Earth Surf. Process. Landf. 41 (9), 1169–1184 doi:.

Ruether, N., Olsen, N.R.B., 2007. Modelling free-forming meander evolution in a laboratory channel using three-dimensional computational fluid dynamics. Geomorphology 89 (308–319). https://doi.org/10.1016/j.geomorph.2006.12.009.

Schumm, S.A., Mosley, M.P., Weaver, W.E., 1987. Experimental Fluvial Geomorphology. John Wiley & Sons publishers, USA 0-471-83077-1.

Schuurman, F., Shimizu, Y., Iwasaki, T., Kleinhans, M.G., 2016. Dynamic meandering in response to upstream perturbations and floodplain formation. Geomorphology 253, 94–109. https://doi.org/10.1016/j.geomorph.2015.05.039.

Shields, A., 1936. Use of Dimensional Analysis and Turbulence Research for Sediment Transport. Preussen Research Laboratory for Water and Marine Constructions, 26, Berlin (In German).

da Silva, A.M.F., Ebrahimi, M., 2017. Meandering morphodynamics: insights from laboratory and numerical experiments and beyond. J. Hydraul. Eng. 143 (9), 03117005. https://doi.org/10.1061/(ASCE)HY.1943-7900.0001324.

Slingerland, R., Smith, N.D., 2004. River avulsion and their deposits. Annu. Rev. Earth Planet. Sci. 32, 257–285. https://doi.org/10.1146/annurev.earth.32.101802.120201.

Stoesser, T., Ruehter, N., Olsen, N.R.B., 2010. Calculation of primary and secondary flow and boundary shear stresses in a meandering channel. Adv. Water Resour. 33, 158–170. https://doi.org/10.1016/j.advwatres.2009.11.001.

Sun, J., Lin, B., Yang, H., 2015. Development and application of a braided river model with non-uniform sediment transport. Adv. Water Resour. 81, 62–74. https://doi.org/10.1016/j.advwatres.2014.12.012.

Vázquez-Tarrío, D., Borgniet, L, Liébault, F., Recking, A., 2017. Using UAS optical imagery and SfM photogrammetry to characterize the surface grain size of gravel bars in a braided river (Vénéon River, French Alps). Geomorphology 285 (2017), 94–105. https://doi.org/10.1016/j.geomorph.2017.01.039.

Williams, R.D., Measures, R., Hicks, D.M., Brasington, J., 2016. Assessment of a numerical model to reproduce event-scale erosion and deposition distributions in a braided river. Water Resour. Res. 52, 6621–6642. https://doi.org/10.1002/2015WR018491.

Wilson, C.A.M.E., Stoesser, T., Olsen, N.R.B., Bates, P.D., 2003. Application and validation of numerical codes in the prediction of compound channel flows. P I Civil Eng-Water 153, 117–128. https://doi.org/10.1680/wame.2003.156.2.117.

Xie, Q., Yang, Y., Lundstrom, T.S., 2019. Field studies of 3D modelling of morphodynamics in a meandering river reach dominated by tides and suspended load. Fluids 4, 15. https://doi.org/10.3390/fluids4010015.

Yang, H., Lin, B., Sun, J., Huang, G., 2017. Simulating laboratory braided rivers with bed-load sediment transport. Water 9, 686. https://doi.org/10.3390/w9090686.

Yang, H., Lin, B., Zhou, J., 2018. Avulsions in a simulated large lowland braided river. Water Resour. Manag. 32, 2301–2314. https://doi.org/10.1007/s11269-018-1930-8.

Zhang, K., Wu, S., Feng, W., Zhang, J., Wen, S., 2020. Bar dynamics in a sandy braided river: insights from sediment numerical simulations. Sediment. Geol., 396 https://doi.org/10.1016/j.sedgeo.2019.105557.

Zinke, P., Olsen, N.R.B., Bogen, J., 2011. 3D numerical modeling of levee depositions in a Scandinavian freshwater delta. Geomorphology 129, 320–333. https://doi.org/10.1016/j.geomorph.2011.02.027.